ADVANCED FUNCTIONAL MATERIALS

Supporting Information

for *Adv. Funct. Mater.,* DOI: 10.1002/adfm.202300338

Symmetry-Mismatch-Induced Ferromagnetism in the Interfacial Layers of $CaRuO_3/SrTiO_3$ Superlattices

Wenxiao Shi, Jine Zhang, Xiaobing Chen, Qinghua Zhang, Xiaozhi Zhan, Zhe Li, Jie Zheng, Mengqin Wang, Furong Han, Hui Zhang, Lin Gu, Tao Zhu, Banggui Liu, Yunzhong Chen, Fengxia Hu, Baogen Shen, Yuansha Chen, and Jirong Sun**

Supporting Information for

Symmetry-mismatch-induced ferromagnetism in the interfacial layers of $CaRuO_3/SrTiO_3$ superlattices

Wenxiao Shi†, Jine Zhang†, Xiaobing Chen†, Qinghua Zhang, Xiaozhi Zhan, Zhe Li, Jie Zheng, Mengqin Wang, Furong Han, Hui Zhang, Lin Gu, Tao Zhu, Banggui Liu, Yunzhong Chen, Fengxia Hu, Baogen Shen, Yuansha Chen* and Jirong Sun*

†These authors contributed equally to this work.

*Corresponding author. Email: yschen@iphy.ac.cn (Y.S.C); jrsun@iphy.ac.cn (J.R.S)

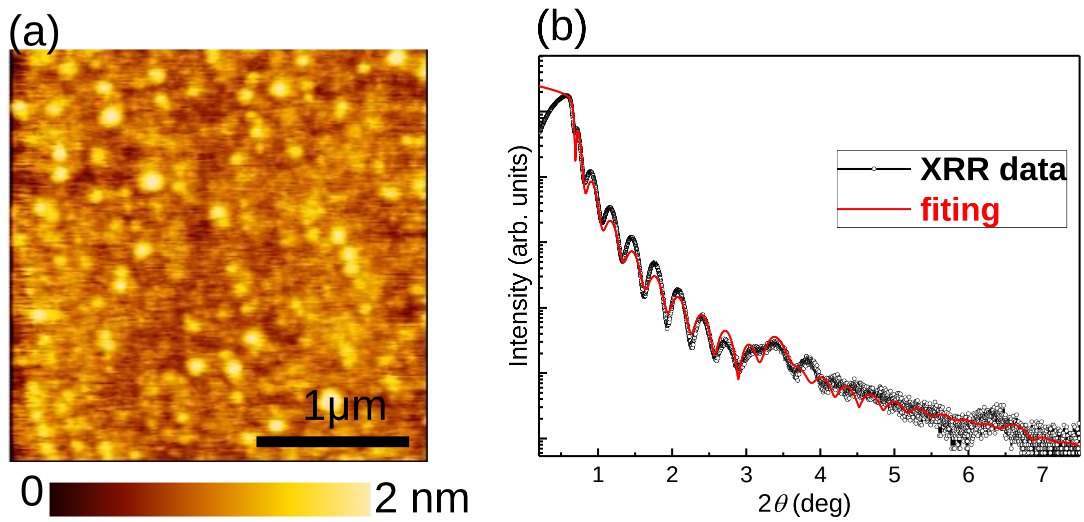

Figure S1. (**a**) Atomic force microscopy topography (3 μm × 3 μm) of $(CRO_6/STO_1)_{10}$ SL on LSAT (001) surface. (**b**) XRR of the $(CRO_6/STO_1)_{10}$ SL grown on the (001)-oriented LSAT substrate. Good agreements between fitting curves (red) and experimental curves (black) are clearly demonstrated. The simulation curve is realized by the commercial software of DIFFRAC^{plus} LEPTOS 7. The deduced thickness of CRO and STO layers is consistent with the targeted structure.

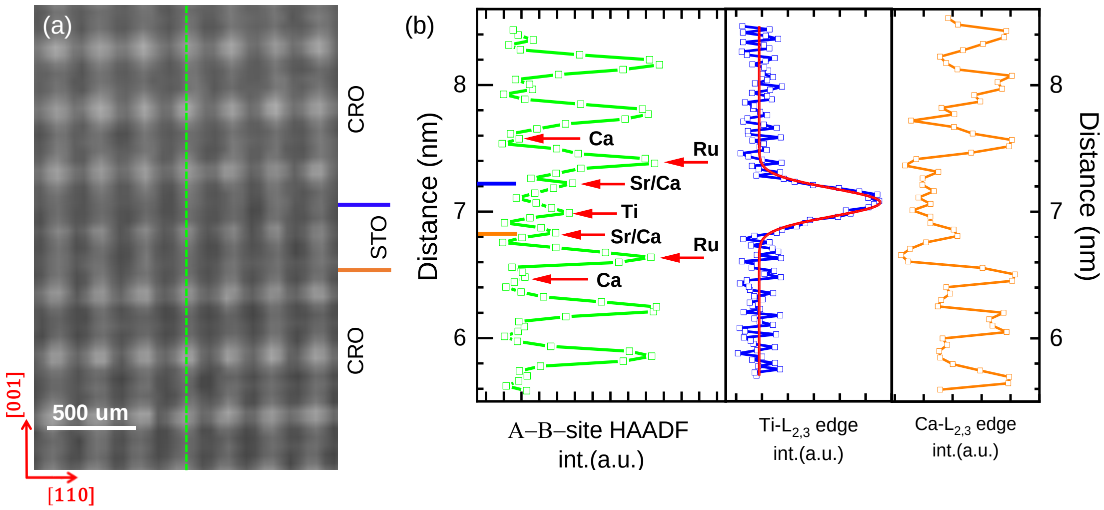

Figure S2. (**a**) Enlarged HAADF image of the a $(CRO_8/STO_1)_{10}$ SL on LSAT. The interfaces between CRO and STO layers are marked by blue and orange horizontal lines. The EELS elemental characterizations are performed along the green line. **(b)** Spatial dependence of the cation HAADF intensity along the vertical direction, and the corresponding Ti $L_{2,3}$ and Ca $L_{2,3}$ edge intensities. The blue and orange horizontal lines in the figure correspond to the lines in (a).

Figure S2 shows the enlarged HAADF image of the CRO/STO interface and corresponding line profiles of the HAADF and EELS intensities, obtained along the vertical direction marked in the image. Identical HAADF intensity is observed for all Ru-sites across the CRO layer, including the Ru-site neighboring STO (Figure S2(b)). This excludes the atomic diffusion between Ru- and Ti-sites at interface. Meanwhile, the EELS result of the Ti-$L_{2,3}$ edge also shows that Ti is strictly localized within the one u.c. STO monolayer (Figure S2(b)), i.e., the atomic diffusion from the Ti- to Ru-sites does not occur. Therefore, Ru-Ti intermixing is negligibly small. The HAADF intensity is also a constant for all Ca-sites (A sites) across the CRO layer, except for the interfacial sites neighboring TiO_2 plane. At the interfacial A-sites, the HAADF intensity is considerably higher than elsewhere. Combining with the Ca-$L_{2,3}$ edge EELS result, we can get the conclusion that the interfacial A-sites are occupied by both Sr and Ca. It should be noticed that, $Sr_{1-x}Ca_xTiO_3$, the possible insert layer caused by such intermixing, is still a nonmagnetic insulator.

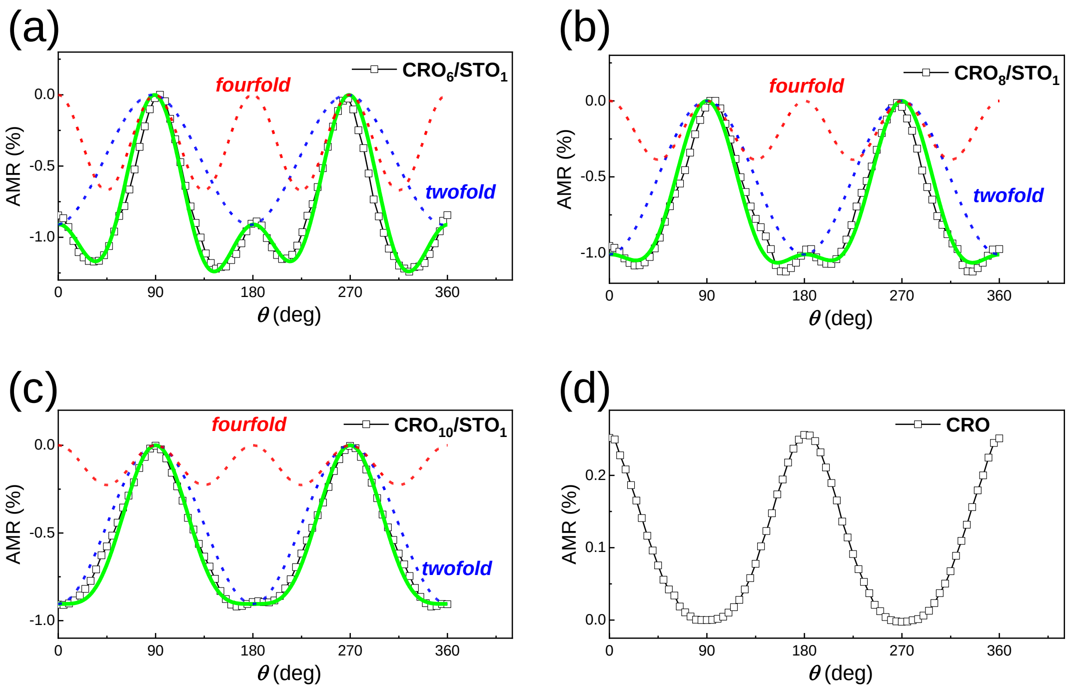

Figure S3. (a)-(c) Angle dependence of the AMR measured at 2 K and 10 T for the $(CRO_6/STO_1)_{10}$ SL (a), $(CRO_8/STO_1)_{10}$ SL (b) and $(CRO_{10}/STO_1)_{10}$ SL (c) on LSAT substrate. The experimental data (black symbols) can be well described by $\mathrm{AMR}(\theta) = c_2 \times \cos(2\theta - \omega_2) + c_4 \times \cos(4\theta - \omega_4)$ with two contributions of fourfold (red curve) and twofold (blue curve) symmetries, where c_2 and c_4 are the amplitudes of AMR contributions with two-fold and four-fold symmetries. Green lines are the results of curve-fitting. Satisfactory agreement with experiment results is obtained adopting suitable fitting parameters. **(d)** In-plane AMR for a CRO bare film on LSAT substrate, presenting the twofold symmetry.

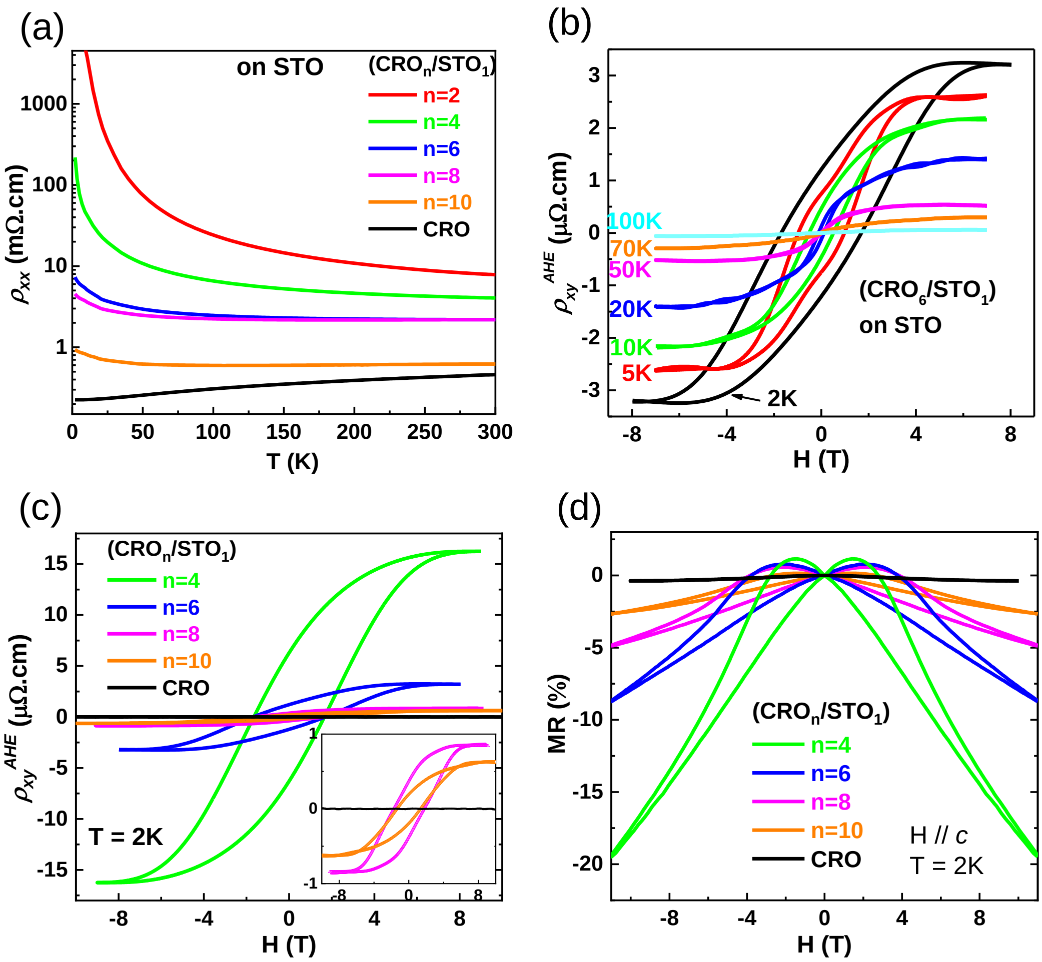

Figure S4. (**a**) Temperature dependence of the resistivity of $(CRO_n/STO_1)_{10}$ SLs grown on STO substrates. (**b**) Magnetic field dependence of the anomalous Hall resistivity of a $(CRO_6/STO_1)_{10}$ SL grown on STO, measured at the temperature from 2 K to 100 K. (**c**) Magnetic field dependence of anomalous Hall resistivity for the $(CRO_n/STO_1)_{10}$ SLs on STO, measured at 2 K. Insert is the enlarged ρ_{xy}^{AHE}-H curves for the CRO_8/STO_1 and CRO_{10}/STO_1 SLs. (**d**) Magnetoresistance as a function of magnetic field for the $(CRO_n/STO_1)_{10}$ SLs on STO, measured at 2 K with the applied field along the out-of-plane direction. The corresponding data of a bare CRO film (50 uc in thickness) is also presented for comparison.

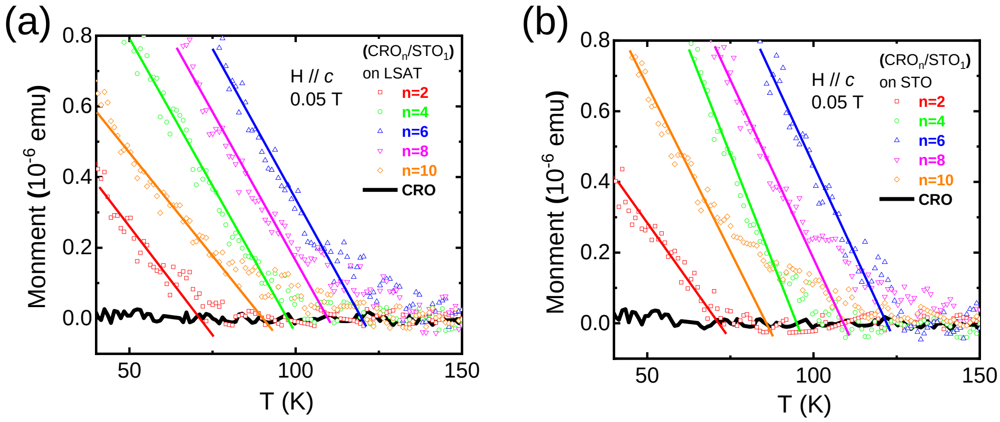

Figure S5. Enlarged M-T curves for $(CRO_n/STO_1)_{10}$ SLs on **(a)** LSAT and **(b)** STO, measured with an out-of-plane field of 0.05 T in field-cooling mode. T_C is deduced for each CRO/STO SL, using the zero-crossing temperature of the tangent line.

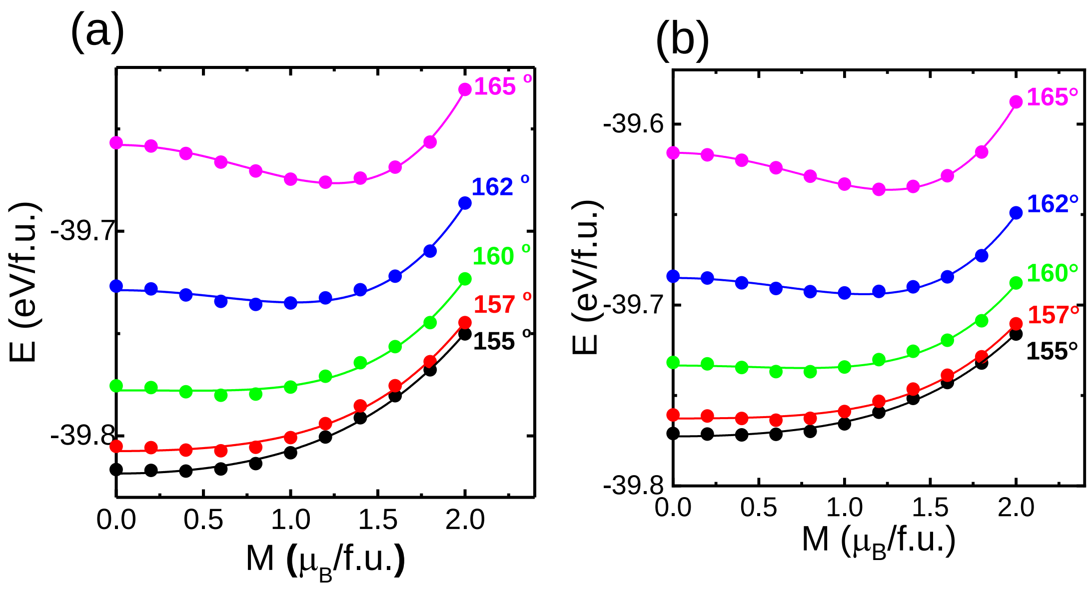

Figure S6. (**a**) The *E-M* relations calculated with different $\beta_{Ru\text{-}O\text{-}Ru}$ angles for CRO on LSAT and (**b**) STO substrate. Fitting the *E-M* relation by $E = a_0 + \frac{a_2}{2}M^2 + \frac{a_4}{4}M^4$, the Stoner parameter I then can be deduced from the coefficient a_2, adopting the relation a_2=[1/N(E_F)-I]/2. The CRO unit cells are constructed using the experimental lattice constants and varied tilting angle $\beta_{Ru\text{-}O\text{-}Ru}$, adopting the biaxial strain state imposed by the LSAT or STO substrate. As local density approximation (LDA) generally underestimates the lattice constants of substrates by 1%,[1] the in-plane lattice constants for the *Pbnm* unit cell on LSAT were set to $a = b = 5.415$ Å ($\sqrt{2}a_{\rm LSAT}\times0.99$, where $a_{\rm LSAT}$= 3.868 Å), the out-of-plane lattice constant was set to $c = 7.68$ Å ($2c_{\rm exp}\times0.99$, where $c_{\rm exp}$= 3.88 Å). The in-plane lattice constants for the *Pbnm* unit cell on STO were set to $a = b = 5.467$ Å ($\sqrt{2}a_{\rm STO}\times0.99$, where $a_{\rm STO}$= 3.905 Å), the out-of-plane lattice constant was set to $c = 7.72$ Å ($2c_{\rm exp}\times0.99$, where $c_{\rm exp}$= 3.86 Å). And the tilting angle $\beta_{Ru\text{-}O\text{-}Ru}$ was set to five different values from 165° to 155°.

Tables S1. (a) The CRO unit cells are constructed using varied tilting angle $\beta_{Ru\text{-}O\text{-}Ru}$, adopting the biaxial strain state imposed by the LSAT substrate. Table lists the calculation results of *$N(E_F)$*, Stoner criterion and effect moment for each model.

$\beta_{Ru\text{-}O\text{-}Ru}$	$N(E_F)$	$IN(E_F)$	M (μB/f.u.)	E_{NM}-E_{FM} (meV/f.u.)	Mag
155	2.33	0.912	-	0.780	PM
157	2.42	0.950	-	2.215	PM
160	2.53	1.015	0.461	4.808	FM
162	2.66	1.122	0.581	8.927	FM
165	2.72	1.260	0.805	19.258	FM

(**b**) The CRO unit cells are constructed using varied tilting angle $\beta_{Ru\text{-}O\text{-}Ru}$, adopting the biaxial strain state imposed by the STO substrate. Table lists the calculation results of *$N(E_F)$*, Stoner criterion and effect moment for each model.

$\beta_{Ru\text{-}O\text{-}Ru}$	$N(E_F)$	$IN(E_F)$	M (μB/f.u.)	E_{NM}-E_{FM} (meV/f.u.)	Mag
155	2.44	0.941	-	0.780	PM
157	2.50	0.981	-	2.918	PM
160	2.60	1.048	0.495	5.528	FM
162	2.65	1.153	0.686	9.207	FM
165	2.59	1.268	0.845	20.284	FM

References

[1] Weber, M. C.; Guennou, M.; Dix, N.; Pesquera, D.; Sánchez, F.; Herranz, G.; Fontcuberta, J.; López-Conesa, L.; Estradé, S.; Peiró, F.; Iñiguez, J.; Kreisel, J. Multiple strain-induced phase transitions in $LaNiO_3$ thin films. *Phys. Rev. B* **2016,** *94,* 014118.